Report

Current Biology

Notch-mediated re-specification of neuronal identity during central nervous system development

Highlights

- Spontaneous fate reprogramming in the *vsx1* lineage of the zebrafish retina
- Nascent *vsx1* bipolar cells are re-specified to an amacrine cell fate
- Notch signaling plays a major role in *vsx1* bipolar cell re-specification
- Over-stimulating Notch signaling enhances reprogramming in the *vsx1* lineage

Authors

Peter Engerer, Eleni Petridou, Philip R. Williams, ..., Ruben Portugues, Thomas Misgeld, Leanne Godinho

Correspondence

leanne.godinho@tum.de

In brief

Engerer, Petridou et al. find evidence for spontaneous cell fate reprogramming during retinal development. Newly post-mitotic *vsx1* bipolar cells switch to an amacrine cell fate. Notch signaling plays a major role, conferring plasticity to nascent bipolar cells, allowing suitable transcription factors to instruct the amacrine cell fate.

Engerer et al., 2021, Current Biology *31*, 4870–4878
November 8, 2021
https://doi.org/10.1016/j.cub.2021.08.049

CellPress

CellPress
OPEN ACCESS

Current Biology

Report

Notch-mediated re-specification of neuronal identity during central nervous system development

Peter Engerer,[1,7,8] Eleni Petridou,[1,2,7] Philip R. Williams,[1,9] Sachihiro C. Suzuki,[3,10] Takeshi Yoshimatsu,[3,11] Ruben Portugues,[4,6] Thomas Misgeld,[1,5,6] and Leanne Godinho[1,12,*]

[1]Institute of Neuronal Cell Biology, Technische Universität München, Biedersteiner Strasse 29, 80802 Munich, Germany
[2]Graduate School of Systemic Neurosciences (GSN), Ludwig-Maximilian University of Munich, Großhaderner Strasse 2, 82152 Planegg-Martinsried, Germany
[3]Department of Biological Structure, University of Washington, 1959 NE Pacific Street, Seattle, WA 98195, USA
[4]Institute of Neuroscience, Technische Universität München, Biedersteiner Strasse 29, 80802 Munich, Germany
[5]German Center for Neurodegenerative Diseases (DZNE), Feodor-Lynen-Strasse 17, 81377 Munich, Germany
[6]Munich Cluster of Systems Neurology (SyNergy), Feodor-Lynen-Strasse 17, 81377 Munich, Germany
[7]These authors contributed equally
[8]Present address: Leica Microsystems CMS GmbH, Am Friedensplatz 3, 68165 Mannheim, Germany
[9]Present address: John F. Hardesty, MD, Department of Ophthalmology and Visual Sciences, Department of Neuroscience, Hope Center for Neurological Disorders, Washington University School of Medicine, St. Louis, MO 63110, USA
[10]Present address: TLO-KYOTO, International Science Innovation Building, Kyoto University, Yoshida Honmachi, Sakyo-ku, Kyoto 606-8501, Japan
[11]Present address: Sussex Neuroscience, School of Life Sciences, University of Sussex, Brighton BN1 9QG, UK
[12]Lead contact
*Correspondence: leanne.godinho@tum.de
https://doi.org/10.1016/j.cub.2021.08.049

SUMMARY

Neuronal identity has long been thought of as immutable, so that once a cell acquires a specific fate, it is maintained for life.[1] Studies using the overexpression of potent transcription factors to experimentally reprogram neuronal fate in the mouse neocortex[2,3] and retina[4,5] have challenged this notion by revealing that post-mitotic neurons can switch their identity. Whether fate reprogramming is part of normal development in the central nervous system (CNS) is unclear. While there are some reports of physiological cell fate reprogramming in invertebrates,[6,7] and in the vertebrate peripheral nervous system,[8] endogenous fate reprogramming in the vertebrate CNS has not been documented. Here, we demonstrate spontaneous fate re-specification in an interneuron lineage in the zebrafish retina. We show that the *visual system homeobox 1* (*vsx1*)-expressing lineage, which has been associated exclusively with excitatory bipolar cell (BC) interneurons,[9–12] also generates inhibitory amacrine cells (ACs). We identify a role for Notch signaling in conferring plasticity to nascent *vsx1* BCs, allowing suitable transcription factor programs to re-specify them to an AC fate. Overstimulating Notch signaling enhances this physiological phenotype so that both daughters of a *vsx1* progenitor differentiate into ACs and partially differentiated *vsx1* BCs can be converted into ACs. Furthermore, this physiological re-specification can be mimicked to allow experimental induction of an entirely distinct fate, that of retinal projection neurons, from the *vsx1* lineage. Our observations reveal unanticipated plasticity of cell fate during retinal development.

RESULTS AND DISCUSSION

Vsx1 progenitors generate bipolar cells (BCs) and amacrine cells (ACs)

Vsx1 is a key determinant of BC fate across vertebrate species.[9–11,13] In the zebrafish retina, *vsx1* BCs are generated by *vsx1* progenitors via terminal, symmetric mitotic divisions,[14,15] suggesting they are hard-wired to the BC fate. However, in a *vsx1*:GFP transgenic line that faithfully reports *vsx1* expression,[12,16] small numbers of ACs are labeled[12] (Figure 1A). We investigated the origin of these ACs by *in vivo* time-lapse recordings in a Gal4-driver line (*Q32*) that provides a lineage label for a subset of *vsx1* cells.[14] ACs were generated by terminally dividing *Q32* progenitors, with BCs as their siblings. These AC-BC divisions represented almost half of all *Q32* divisions (41.2% ± 6%, mean ± SEM, 141 divisions, 16 fish; Figure 1B; see also lineage tracing studies[17,18]). *Q32* daughters that became ACs maintained somal contact with their BC sibling for several hours (5.3 ± 0.7 h, mean ± SEM, 13 pairs, 6 fish), before acquiring AC features. By contrast, BC-BC siblings did not lose somal contact after mitosis (at least over the recording, 14.5 ± 0.7 h, mean ± SEM, 10 pairs, 7 fish). Loss of somal contact with their BC sibling thus represents the earliest sign of morphological differentiation toward an AC fate (Figure S1A). *Q32* ACs express a bona fide pan AC marker, *ptf1a*[19]

CellPress
OPEN ACCESS

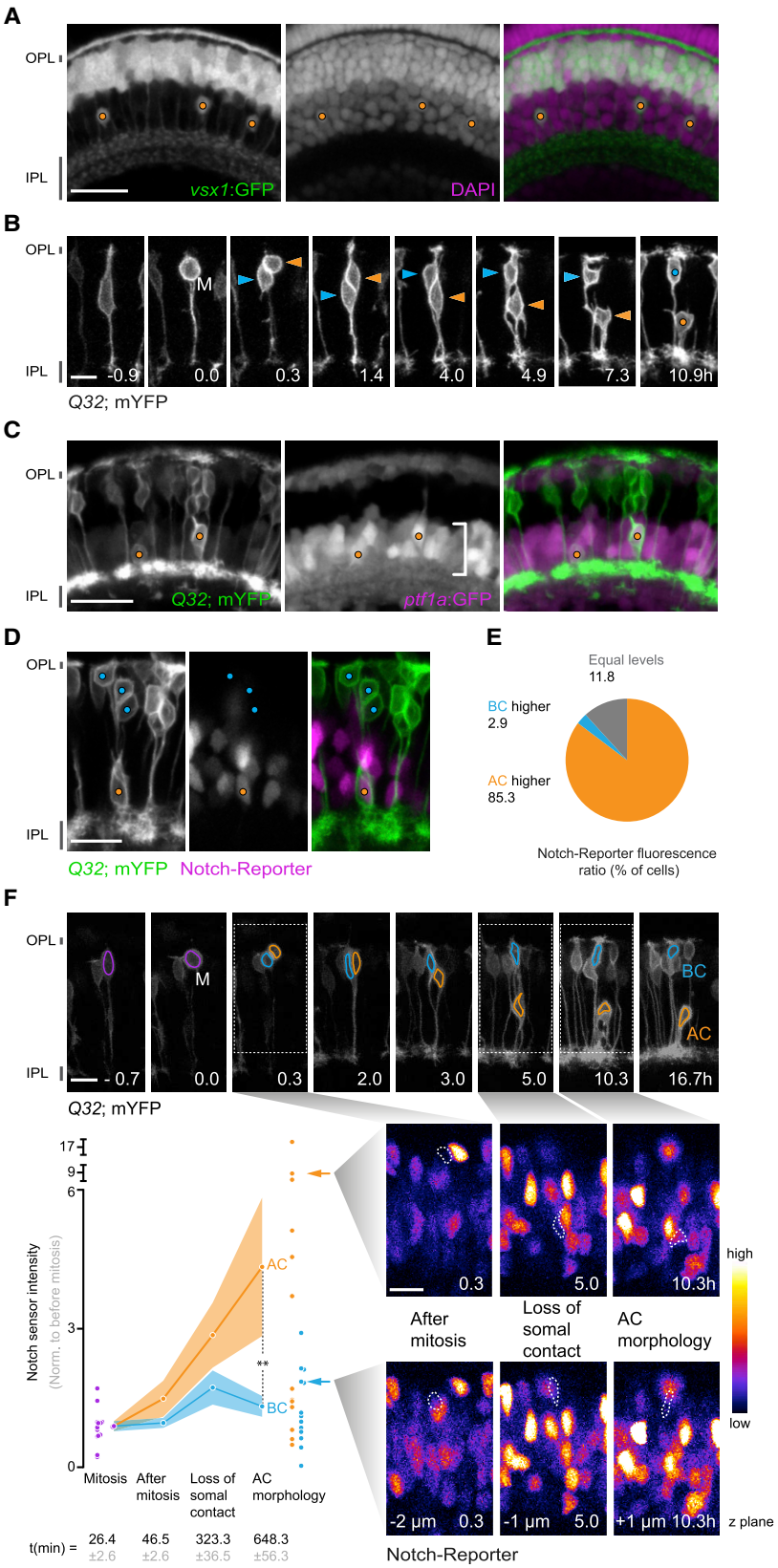

Figure 1. *Vsx1* progenitors generate ACs

(A) 3 dpf *vsx1*:GFP retina with *vsx1*$^{+}$ BCs and ACs (orange circles).

(B) 2 dpf *Q32* progenitor undergoing mitosis (M), generates a BC (cyan arrowhead; circle, final time point) and an AC (orange arrow-head, circle final time-point).

(C) 3 dpf WT retina showing *ptfa*:GFP^{+} *Q32* ACs (orange circles). *Ptf1a*:GFP labels all ACs (INL, bracket, center panel). *Ptf1a*-GFP signal bleeds through *Q32*-YFP channel.

(D) 3 dpf retina showing Notch-reporter (*tp1*:hmgb1mCherry) expression in a *Q32* AC (orange circle), but not in surrounding *Q32* s BCs (cyan circles).

(E) Notch-reporter (*tp1*:hmgb1mCherry) fluorescence intensity in *Q32* ACs and BCs. AC and BC categories were tested against an expected frequency of 50% using a binomial test, $p < 0.0001$; 30 cells, 10 fish. Four ACs (of 34) displayed equal levels of fluorescence as neighboring BCs.

(F) 2 dpf transgenic retina (*Q32*; mYFP; *tp1*:H2BmCherry; top grayscale images, gamma adjusted) showing a WT *Q32* progenitor (purple outline) generating a BC (cyan) and an AC (orange). Notch-reporter levels in the AC and BC depicted using a Fire LUT (below, right). Notch-reporter intensity levels (means ± SEMs) for 13 *Q32* progenitors (8 fish) and their BC (cyan) and AC (orange) daughters (below, left). Times in relation to the time point before mitosis. Significant differences between BC-AC pairs were found when the AC acquired its characteristic morphology (Wilcoxon matched-pairs signed-rank test, $p = 0.0061$).

Scale bars, 20 µm (A and C); 10 µm (B, D, and F). IPL, inner plexiform layer; OPL, outer plexiform layer.

See also Figures S1A, S2, and S3A–S3C.

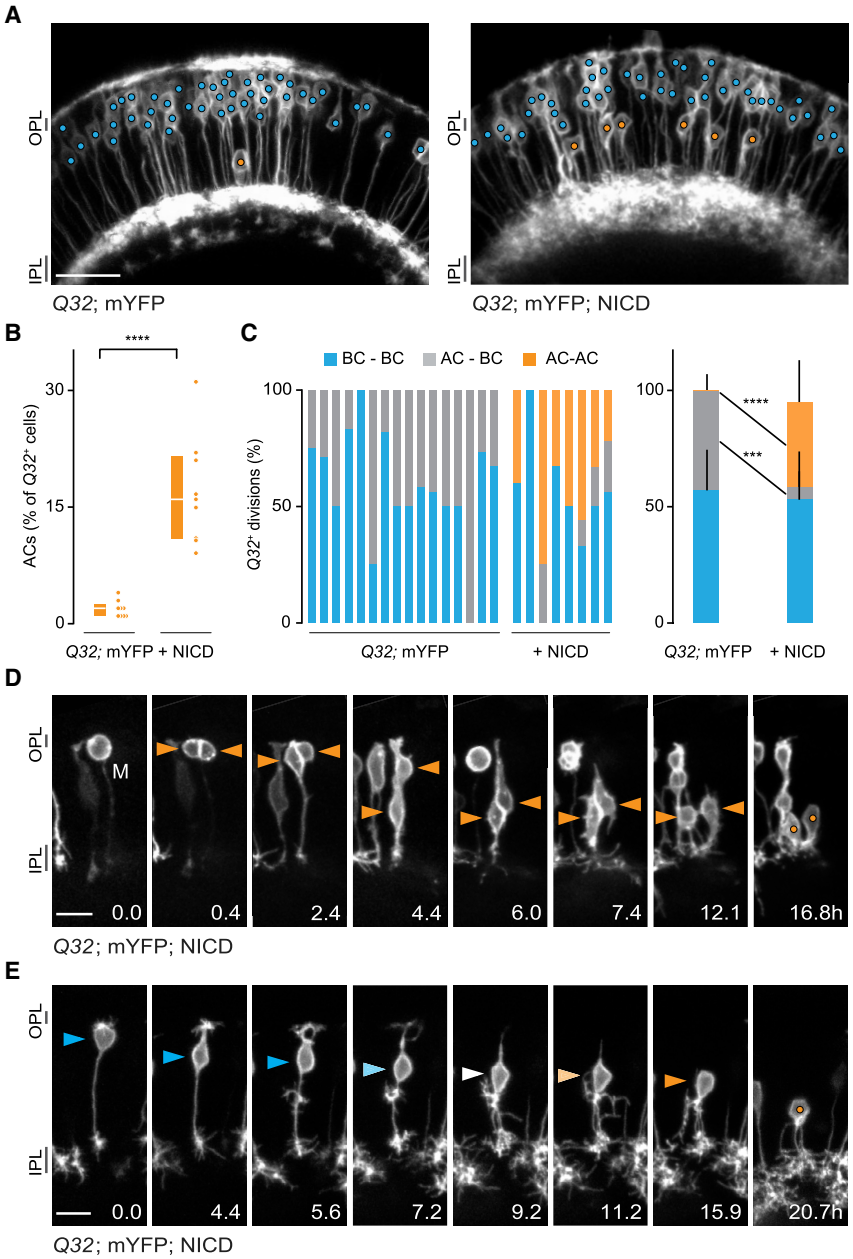

Figure 2. Notch signaling promotes AC fate in the *vsx1* lineage

(A) 3 dpf retinae from *Q32* WT and *Q32* NICD. BCs (cyan circles), ACs (orange circles).

(B) Proportion of ACs in WT and *Q32* NICD. Median and interquartile range (IQR) shown. *Q32* WT (21 ACs, 9 fish); *Q32* NICD (140 ACs, 9 fish), $p < 0.0001$, Mann-Whitney U test.

(C) Proportion of *Q32* divisions in WT and following NICD OE for each fish (left). Collective representation of *Q32* divisions, representing median and IQR per group (right). BC-BC: *Q32* WT versus NICD, $p = 0.5134$. AC-BC: *Q32* WT versus NICD, $p = 0.0004$. AC-AC: *Q32* WT versus NICD, $p < 0.0001$. WT: 141 *Q32* divisions, 16 fish; *Q32* NICD: 44 divisions, 8 fish. Mann-Whitney U test.

(D) 2 dpf *Q32* NICD retina, showing a mitotic progenitor (M) generating 2 ACs (orange arrowheads; circles, last time point).

(E) 2 dpf *Q32* NICD retina, showing a BC (cyan arrowhead), transdifferentiating into an AC (orange arrowhead; circle, last time point).

Scale bars, 20 μm (A); 10 μm (D and E).

See also Figures S1, S3D, and S3E.

(99.2% ± 0.8% of *Q32* ACs were *ptf1a*:GFP$^+$; mean ± SEM, 60 cells, 13 fish; Figure 1C), and only a small number maintain *vsx1* expression (1 of 26 *Q32* ACs was *vsx1*:GFP$^+$ at 3 days post-fertilization [dpf], 15 fish; Figures S2A–S2C), accounting for the low AC number in *vsx1*:GFP retinae (0.8% ± 0.2% of 2,295 *vsx1*:GFP$^+$ cells, mean ± SEM, 3 dpf, 8 fish). We also detected cells with an AC morphology in BC transgenic lines (*crx*:mCFP and *ctbp2*:mEGFP;[14,20,21] Figure S2D), hinting at their BC lineage origin.

Notch signaling promotes the AC fate in the *vsx1* lineage

To investigate whether Notch signaling underlies the asymmetric fates,[16,22–26] we crossed the *Q32* line to Notch-reporter lines[27,28] (Figure 1D). The majority of *Q32* ACs displayed higher Notch-reporter levels than *Q32* BCs in their vicinity (Figure 1E). To determine when the divergence of Notch signaling emerged, we monitored Notch-reporter expression in time-lapse recordings (Figure 1F). Notch-reporter levels were low in *Q32* progenitors and increased gradually post-mitosis. Significant increases were only detectable in the AC sibling of AC-BC pairs when it acquired its typical morphology (average 10 h post-mitosis), implicating the post-mitotic nature of this signaling event. We investigated whether mechanisms at the progenitor level[29–31] accounted for the signaling asymmetry in the ensuing daughters. However, we found neither asymmetric distribution of the Notch regulator Numb (10 cells, 4 fish) nor mitotic cleavage along a stereotypic axis (45 cells, 25 fish; Figures S3A and S3B), suggesting these key players are not involved.

We used DAPT, a γ-secretase inhibitor, to abrogate Notch signaling[32] and found an ~50% decrease in *vsx1*:GFP$^+$ ACs (DAPT-treated 2.0 ± 1.4 ACs per region, 23 regions, 12 fish versus DMSO controls 5.0 ± 1.6 ACs per region, 18 regions, 9 fish, median ± SD, $p < 0.0001$, Mann-Whitney U test; Figure S3B). Conversely, overexpression (OE) of the Notch intracellular domain (NICD)[33] in the *vsx1* lineage (*Q32* NICD) led to a 9-fold increase in *Q32* ACs (Figures 2A and 2B), that persisted at least until 5 dpf (Figure S3C). The increased AC number did not arise from increased *Q32* progenitor proliferation (0.21 ± 0.03 wild type [WT] versus 0.19 ± 0.05 NICD, means ± SEMs, divisions per hour, monitored 18 h from 2 to 3 dpf; $p = 0.75$, t test), but rather from the emergence of AC-AC pairs, a division mode not seen in *Q32* WT (Figures 2C and 2D), and by BC-to-AC

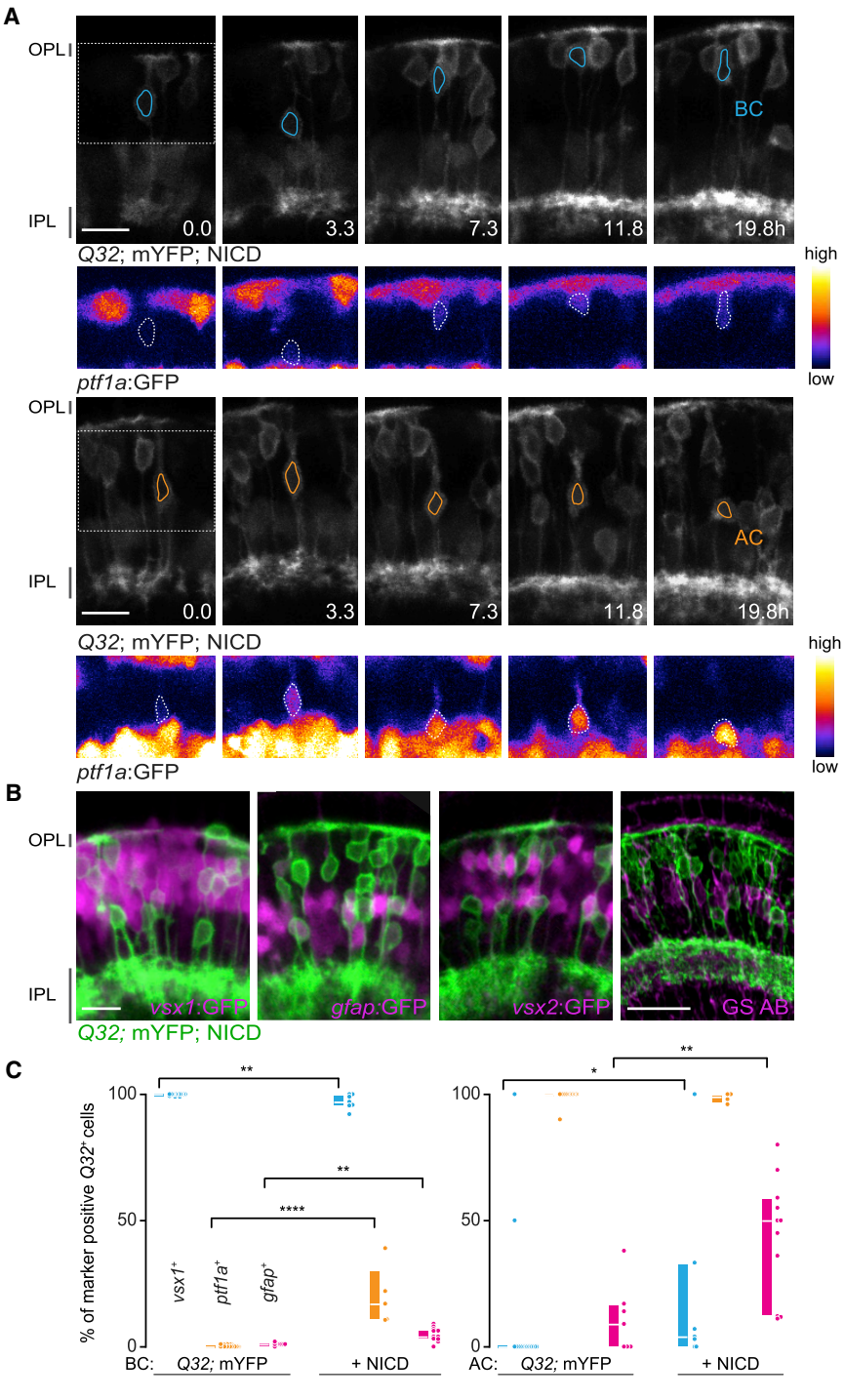

Figure 3. Marker expression in re-specified ACs

(A) In *Q32* NICD, BCs (outlined cyan, upper grayscale panels), express *ptf1a*:GFP (Fire LUT), albeit at lower levels than in ACs (outlined orange, lower grayscale panels). *Ptf1a*-GFP signal bleeds through *Q32*-YFP channel (grayscale panels).

(B) Following NICD OE, transdifferentiated *Q32* ACs do not express *vsx1*:GFP but *gfap*:GFP. *Q32* ACs are negative for *vsx2*:GFP and glutamine synthetase (GS antibody, AB).

(C) Percentage of *Q32* BCs (left) and ACs (right) expressing *vsx1*, *ptf1a* and *gfap* in WT or *Q32* NICD. Median and IQR represented. BCs: *vsx1*:GFP$^+$: *Q32* WT, (1227 BCs, 14 fish) versus NICD, (416 BCs, 7 fish); p = 0.0034. *Ptf1a*:GFP$^+$: *Q32* WT (1,614 BCs, 14 fish) versus NICD (486 BCs, 5 fish); p < 0.0001. *Gfap*:GFP$^+$: *Q32* WT (718 BCs, 7 fish) versus NICD (984 BCs, 11 fish); p = 0.0022. ACs: *vsx1*:GFP$^+$: *Q32* WT (28 ACs, 15 fish) versus *Q32* NICD (100 ACs, 7 fish); p = 0.0129. *Ptf1a*:GFP$^+$: *Q32* WT (60 ACs, 13 fish) versus *Q32* NICD (124 ACs, 4 fish); p = 0.1206. *Gfap*:GFP$^+$: *Q32* WT (43 ACs, 7 fish) versus *Q32* NICD (335 ACs, 11 fish); p = 0.0078. Mann-Whitney U test for pairwise comparisons.

Scale bars, 10 μm (A and B).

transdifferentiation (17 observations, 9 fish; Figure 2E). Transdifferentiating BCs exhibited process exuberance and took longer to acquire AC features compared to WT (Figure S1B), highlighting the fate switch that occurred along their original differentiation trajectory. Time-lapse of the Notch-reporter in *Q32* NICD during transdifferentiation showed that Notch signaling increases when the soma translocated toward the inner part of the inner nuclear layer (INL) and AC morphology emerged. Following AC-BC divisions, Notch-reporter levels increased significantly in the AC sibling several hours (average 6 h) post-mitosis (Figures S1C and S1D). Thus, also after NICD OE, Notch signaling appears to operate post-mitotically to re-specify fate.

Transdifferentiated ACs lose BC markers and express markers of immaturity

ACs in *Q32* NICD retinae were *ptf1a*:GFP$^+$ and most lost expression of *vsx1*:GFP (Figures 3A and 3C). The NICD-induced ACs also lacked other BC markers (0% *crx*:mCFP$^+$, 65 ACs, 3 fish; 1.9% ± 1.1% *ctbp2*:mEGFP$^+$, means ± SEMs, 95 ACs, 4 fish), resembling WT *Q32* ACs. Notably, 20% of BCs in *Q32* NICD expressed *ptf1a*:GFP, a phenotype that is absent in WT fish (Figures 3A and 3C). This suggests that after NICD OE, some BCs expressed AC markers, but did not adopt an AC morphology. Moreover, >40% of *Q32* NICD ACs were *gfap*:GFP$^+$, which is expressed in neural progenitors[34,35] (Figures 3B and 3C). Importantly, ~11% of WT *Q32* ACs also expressed this marker. Notch signaling is associated with Müller cell specification[36–39] and GFAP is expressed by Müller glia.[34] To exclude that NICD-induced *Q32* ACs were driven toward a Müller cell fate, we examined their expression of glutamine synthetase (GS)[40] and *vsx2*,[12] but found no evidence for this (GS: 0 of 68 ACs, 7 *Q32* NICD fish; 0 of 28 ACs, 9 *Q32* WT fish; *vsx2*:GFP: 0 of 274 ACs, 6 *Q32* NICD fish; 0 of 26 ACs, 6 *Q32* WT fish). Thus, *gfap*

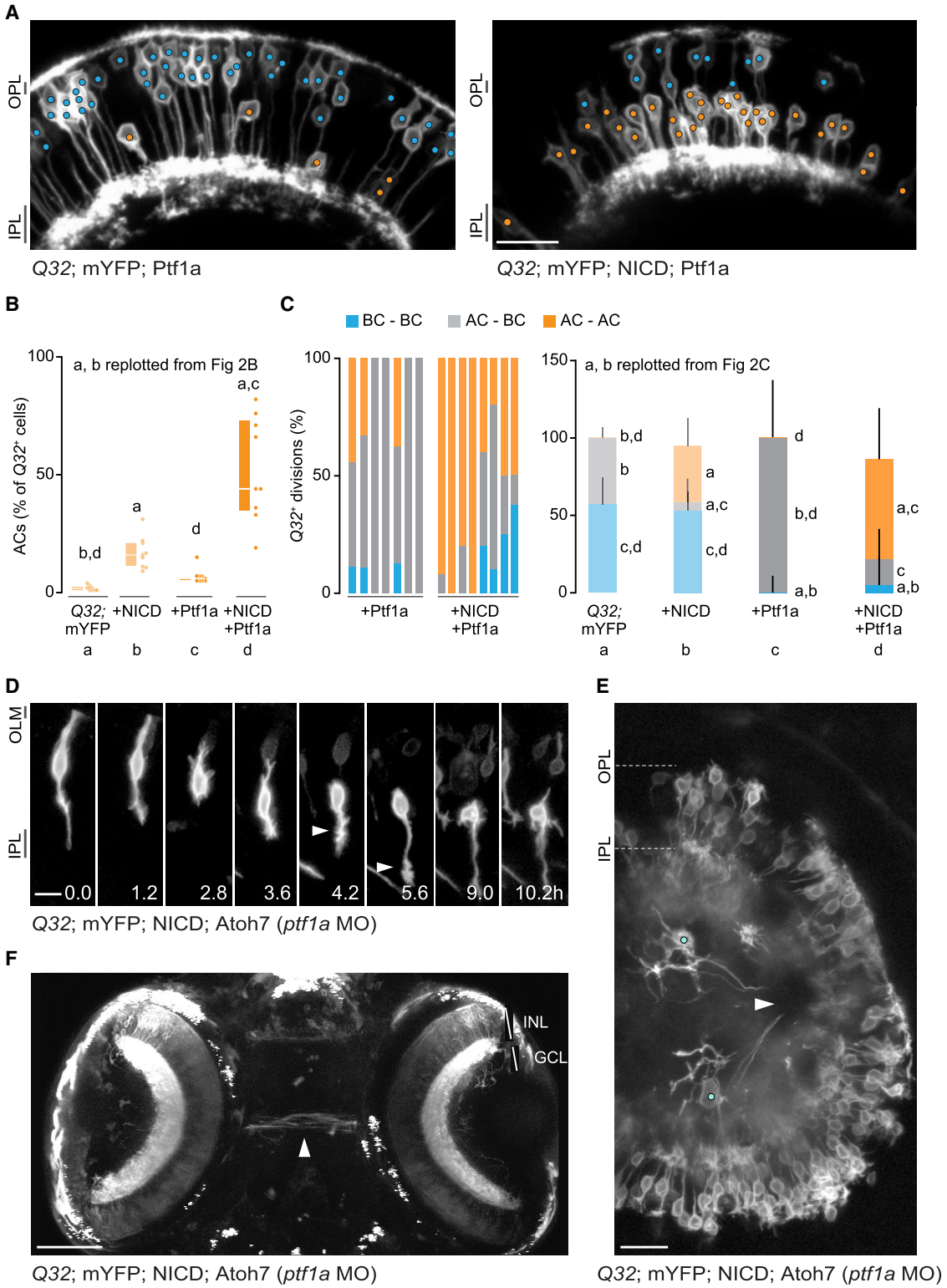

Figure 4. Notch signaling imparts plasticity to nascent post-mitotic cells

(A) 3 dpf retinae from *Q32* Ptf1a and *Q32* NICD Ptf1a fish. *Q32* BCs (cyan circles), ACs (orange circles).

(B) Proportion of ACs in *Q32* Ptf1a and *Q32* NICD Ptf1a represented as median and IQR. *Q32* Ptf1a (66 ACs, 9 fish), *Q32* NICD Ptf1a (372 ACs, 9 fish). *Q32* WT and *Q32* NICD originally plotted in Figure 2B. Significant differences found between WT and NICD ($p = 0.0003$), WT and NICD Ptf1a ($p < 0.0001$), and Ptf1a and NICD

(legend continued on next page)

in *Q32* ACs does not indicate Müller cell identity, but rather an immature state, permissive of a fate switch.

Ptf1a can induce the AC fate in the *vsx1* lineage

We next asked whether Ptf1a, a determinant of AC fate,[41–45] also governs the fate of *vsx1* ACs. Ptf1a OE in the *vsx1* lineage (*Q32* Ptf1a) resulted in a 3.6-fold increase in *Q32* ACs compared to WT (Figures 4A and 4B). Divisions generating at least 1 AC were higher in *Q32* Ptf1a (100% ± 6.19%, median ± SD) than in *Q32* WT (43% ± 23.8%, median ± SD, Mann-Whitney U test, p = 0.0001; Figure 4C) and in *Q32* NICD (47% ± 28.5%, median ± SD, Mann-Whitney U test, p = 0.0048). Surprisingly, we found a lower number of excess ACs in *Q32* Ptf1a compared to *Q32* NICD (Figure 4B), likely due to the lack of transdifferentiation events. Thus, Ptf1a appears to influence fate around mitosis or shortly thereafter. To examine whether NICD OE could extend this plasticity window, we generated *Q32* NICD Ptf1a fish and found a 28-fold increase in *Q32* ACs compared to WT (Figures 4A and 4B). AC-AC pairs accounted for the majority of divisions in these fish (66.5%; Figure 4C). Thus, physiological Notch signaling confers plasticity to nascent *vsx1* BCs, making them receptive to Ptf1a, which instructs the switch to an AC fate, a phenomenon that can be enhanced by combined NICD and Ptf1a OE. We next probed whether NICD OE combined with another transcription factor could instruct a cell fate beyond ACs.

Ganglion cell (GC)-like cells can be induced in the *vsx1* lineage

We tested whether GCs could be generated by knocking down *ptf1a*[43,46] to suppress AC fate and overexpressing NICD with atonal homolog 7 (Atoh7), a critical GC fate determinant.[47–51] We observed bipolar-shaped *Q32* cells, transforming morphologically while translocating to the GC layer (GCL) and initiating axon outgrowth (14 cells, 3 fish; Figure 4D). These cells expressed *isl2b*:GFP, a GC marker[52] (Figure S4). Of 68 *Q32* GCL-localized cells (24 fish), 30 bore morphologies reminiscent of GCs (Figure 4E), while the rest lacked a detectable axon or displayed few or no discernible neurites. At 5 dpf (4 fish), we observed *Q32* GC axons at the optic chiasm, suggesting successful retinal exit and path finding en route to the optic tectum (Figures 4F and S4).

Implications of developmental plasticity

Here, we report physiological Notch-dependent fate reprogramming in the *vsx1* lineage, allowing nascent BCs to re-specify to an AC fate. That Notch signaling confers plasticity to nascent post-mitotic cells has been suggested to occur in the postnatal mouse retina.[53] Notch signaling has also been implicated in transdifferentiation events in the damaged mammalian cochlea.[54] In the latter case, however, in contrast to our findings, attenuation of Notch signaling is involved.[55]

Vsx1-lineage-derived ACs represent a small fraction of the total AC population, the majority of which arise from a different lineage.[43,56] Could *vsx1* ACs have a specific functional significance? One can speculate that *vsx1* ACs are generated "on demand," with the BC-to-AC re-specification allowing local fine-tuning of excitation and inhibition. Reducing the AC number, using a *ptf1a* morpholino, led to an almost 2-fold increase in *vsx1* cells expressing *ptf1a*:GFP, thus commencing differentiation toward an inhibitory fate.

Finally, understanding the mechanisms of physiological fate re-specification could guide cell replacement strategies such as direct *in vivo* reprogramming.[57] While progress has been made converting glia to neurons,[58,59] re-specifying neurons from one subtype to another is limited to a short developmental time window, perhaps due to epigenetic changes that fixate cell type identities.[2,3,5] A pulse of Notch signaling may rejuvenate post-mitotic cells and re-open the window for transcription factor-induced re-specification of neuronal subtypes and thus should be explored in the ongoing search for efficient replacement strategies.

STAR★METHODS

Detailed methods are provided in the online version of this paper and include the following:

- KEY RESOURCES TABLE
- RESOURCE AVAILABILITY
  - Lead Contact
  - Materials Availability
  - Data and Code Availability
- EXPERIMENTAL MODEL AND SUBJECT DETAILS
- METHOD DETAILS
  - Generation of constructs
  - Capped RNA synthesis and injections
  - Mounting zebrafish larvae for *in vivo* imaging
  - *In vivo* imaging
  - Photoconversion

Ptf1a (p = 0.0005), denoted by a (significantly different from *Q32* WT), b (from NICD), c (from Ptf1a), or d (from NICD Ptf1a). Kruskal-Wallis and post hoc Dunn's multiple comparisons test, further adjusted by the Benjamini-Hochberg false discovery rate (FDR) method.

(C) *Q32* divisions in *Q32* Ptf1a and *Q32* Ptf1a NICD for each fish (left). Divisions representing median and IQR per group (right). *Q32* Ptf1a: 42 divisions, 7 fish; *Q32* NICD Ptf1a: 52 divisions, 8 fish. *Q32* WT and *Q32* NICD originally plotted in Figure 2C. Significant differences were found in BC-BC divisions: WT versus Ptf1a (p = 0.0001), WT versus NICD Ptf1a (p = 0.0004), NICD versus Ptf1a (p = 0.0029), NICD versus NICD Ptf1a (p = 0.0075); AC-BC divisions: WT versus NICD (p = 0.0127), NICD versus Ptf1a (p = 0.0001), Ptf1a versus NICD Ptf1a (p = 0.0034); AC-AC divisions: WT versus NICD (p = 0.0007), WT versus NICD Ptf1a (p < 0.0001), Ptf1a versus NICD Ptf1a (p = 0.0035), denoted as in (B). Kruskal-Wallis and post hoc Dunn's multiple comparisons test, further adjusted by the Benjamini-Hochberg FDR method.

(D) An emerging GC-like cell in a 2-dpf *Q32* mYFP NICD Atoh7 retina with *ptf1a* morpholino (MO). The cell migrates basally, loses its bipolar morphology, and grows out an axon (arrowhead) and apically directed processes.

(E) Two *Q32* GC-like cells in a 3-dpf transgenic embryo (*Q32*; mYFP; NICD; Atoh7 and *ptf1a* MO). Putative axons exit the retina (arrowhead). Gamma adjusted.

(F) Dorsal view of a 3-dpf embryo (rostral top, eyes lateral) in which GC-like cells were induced (*Q32*; mYFP; NICD; Atoh7 and *ptf1a* MO), showing axons at the chiasm (arrowhead). Gamma adjusted.

Scale bars, 20 μm (A); 10 μm (D and E); 100 μm (F). GCL, ganglion cell layer; INL, inner nuclear layer; OLM, outer limiting membrane.

See also Figure S4.

- Morpholino injections
- DAPT treatment
- Immunostaining
- Genotyping of Q32 crosses

- QUANTIFICATION AND STATISTICAL ANALYSIS
  - Cell type classification of Q32 cells
  - Quantification of Kaede recovery in photoconverted Q32 cells
  - Analysis of DAPT treated animals
  - Notch-Reporter levels in differentiated Q32 cells
  - Monitoring Notch-Reporter levels in time-lapse recordings of the Q32 lineage
  - Division rate analysis
  - Cleavage plane analysis
  - Statistics

SUPPLEMENTAL INFORMATION

Supplemental information can be found online at https://doi.org/10.1016/j.cub.2021.08.049.

ACKNOWLEDGMENTS

We thank K. Wullimann for fish husbandry, Y. Hufnagel for technical support, M. Schetterer for administrative support, and S. Vagionitis for critical reading of an earlier version of this manuscript. We are grateful to M. Nonet (Washington University in St. Louis), M. Meyer (King's College London), and J. Clarke (King's College London) for the pCold Heart Tol2 vector, *5xUAS*:TagRFP-T, and PCS2 Numb-GFP vectors, respectively. We thank S. Higashijima (National Institutes of Natural Sciences, Okazaki Institute for Integrative Bioscience) for the Tg(*vsx1*:GFP)nns5 and Tg(*vsx2*:GFP)nns1 BAC transgenic lines. We are very grateful to Rachel Wong (University of Washington, Seattle), who generously supported this project and provided the following transgenic lines: Tg(*14xUAS*:MYFP) and Tg(*crx*:MA-CFP)q20. We thank L. Lagnado (University of Sussex, UK) for the Tg(−1.8ctbp2:gap43-EGFP)lmb1 line. This project was funded by the Deutsche Forschungsgemeinschaft (DFG, German Research Foundation) through SFB870, TP A11, reference number 118803580. Work in L.G.'s and R.P.'s groups is further supported by the DFG through TRR-274, TP C04, Project ID 408885537. T.M. and R.P. are supported by the Munich Center for Systems Neurology (SyNergy; EXC 2145). T.M. is further supported by the German Center for Neurodegenerative Diseases (DZNE Munich). P.E. was supported by the DFG Research Training Group 1373 and the Graduate School of the Technische Universität München (TUM-GS). E.P. is supported by the Elite Network of Bavaria (MSc "Biomedical Neuroscience"). P.R.W. was supported by the Human Frontier Science Program and the Wings for Life Foundation. S.C.S. and T.Y. were supported by a grant awarded to R. Wong (NIH EY14358).

AUTHOR CONTRIBUTIONS

P.E., E.P., P.R.W., T.M., and L.G. conceived of the project and designed the experiments. L.G. and T.M. supervised the project. P.E. and E.P. performed the experiments. P.E., S.C.S., T.Y., and L.G. generated new constructs and transgenic lines. R.P. advised on the data analysis. L.G. wrote the paper, with input from all of the authors.

DECLARATION OF INTERESTS

The authors declare no competing interests.

Received: June 20, 2020
Revised: June 27, 2021
Accepted: August 18, 2021
Published: September 16, 2021

REFERENCES

1. Deneris, E.S., and Hobert, O. (2014). Maintenance of postmitotic neuronal cell identity. Nat. Neurosci. *17*, 899–907.
2. De la Rossa, A., Bellone, C., Golding, B., Vitali, I., Moss, J., Toni, N., Lüscher, C., and Jabaudon, D. (2013). In vivo reprogramming of circuit connectivity in postmitotic neocortical neurons. Nat. Neurosci. *16*, 193–200.
3. Rouaux, C., and Arlotta, P. (2013). Direct lineage reprogramming of post-mitotic callosal neurons into corticofugal neurons in vivo. Nat. Cell Biol. *15*, 214–221.
4. Goodson, N.B., Park, K.U., Silver, J.S., Chiodo, V.A., Hauswirth, W.W., and Brzezinski, J.A., 4th. (2020). Prdm1 overexpression causes a photoreceptor fate-shift in nascent, but not mature, bipolar cells. Dev. Biol. *464*, 111–123.
5. Montana, C.L., Kolesnikov, A.V., Shen, S.Q., Myers, C.A., Kefalov, V.J., and Corbo, J.C. (2013). Reprogramming of adult rod photoreceptors prevents retinal degeneration. Proc. Natl. Acad. Sci. USA *110*, 1732–1737.
6. Richard, J.P., Zuryn, S., Fischer, N., Pavet, V., Vaucamps, N., and Jarriault, S. (2011). Direct in vivo cellular reprogramming involves transition through discrete, non-pluripotent steps. Development *138*, 1483–1492.
7. Sprecher, S.G., and Desplan, C. (2008). Switch of rhodopsin expression in terminally differentiated Drosophila sensory neurons. Nature *454*, 533–537.
8. Wright, M.A., Mo, W., Nicolson, T., and Ribera, A.B. (2010). In vivo evidence for transdifferentiation of peripheral neurons. Development *137*, 3047–3056.
9. Chow, R.L., Snow, B., Novak, J., Looser, J., Freund, C., Vidgen, D., Ploder, L., and McInnes, R.R. (2001). Vsx1, a rapidly evolving paired-like homeobox gene expressed in cone bipolar cells. Mech. Dev. *109*, 315–322.
10. Passini, M.A., Levine, E.M., Canger, A.K., Raymond, P.A., and Schechter, N. (1997). Vsx-1 and Vsx-2: differential expression of two paired-like homeobox genes during zebrafish and goldfish retinogenesis. J. Comp. Neurol. *388*, 495–505.
11. Shi, Z., Trenholm, S., Zhu, M., Buddingh, S., Star, E.N., Awatramani, G.B., and Chow, R.L. (2011). Vsx1 regulates terminal differentiation of type 7 ON bipolar cells. J. Neurosci. *31*, 13118–13127.
12. Vitorino, M., Jusuf, P.R., Maurus, D., Kimura, Y., Higashijima, S., and Harris, W.A. (2009). Vsx2 in the zebrafish retina: restricted lineages through derepression. Neural Dev. *4*, 14.
13. Shi, Z., Jervis, D., Nickerson, P.E., and Chow, R.L. (2012). Requirement for the paired-like homeodomain transcription factor VSX1 in type 3a mouse retinal bipolar cell terminal differentiation. J. Comp. Neurol. *520*, 117–129.
14. Engerer, P., Suzuki, S.C., Yoshimatsu, T., Chapouton, P., Obeng, N., Odermatt, B., Williams, P.R., Misgeld, T., and Godinho, L. (2017). Uncoupling of neurogenesis and differentiation during retinal development. EMBO J. *36*, 1134–1146.
15. Weber, I.P., Ramos, A.P., Strzyz, P.J., Leung, L.C., Young, S., and Norden, C. (2014). Mitotic position and morphology of committed precursor cells in the zebrafish retina adapt to architectural changes upon tissue maturation. Cell Rep. *7*, 386–397.
16. Kimura, Y., Satou, C., and Higashijima, S. (2008). V2a and V2b neurons are generated by the final divisions of pair-producing progenitors in the zebrafish spinal cord. Development *135*, 3001–3005.
17. He, J., Zhang, G., Almeida, A.D., Cayouette, M., Simons, B.D., and Harris, W.A. (2012). How variable clones build an invariant retina. Neuron *75*, 786–798.
18. Wang, M., Du, L., Lee, A.C., Li, Y., Qin, H., and He, J. (2020). Different lineage contexts direct common pro-neural factors to specify distinct retinal cell subtypes. J. Cell Biol. *219*, e202003026.
19. Godinho, L., Mumm, J.S., Williams, P.R., Schroeter, E.H., Koerber, A., Park, S.W., Leach, S.D., and Wong, R.O. (2005). Targeting of amacrine cell neurites to appropriate synaptic laminae in the developing zebrafish retina. Development *132*, 5069–5079.

20. Odermatt, B., Nikolaev, A., and Lagnado, L. (2012). Encoding of luminance and contrast by linear and nonlinear synapses in the retina. Neuron *73*, 758–773.

21. Suzuki, S.C., Bleckert, A., Williams, P.R., Takechi, M., Kawamura, S., and Wong, R.O. (2013). Cone photoreceptor types in zebrafish are generated by symmetric terminal divisions of dedicated precursors. Proc. Natl. Acad. Sci. USA *110*, 15109–15114.

22. Batista, M.F., Jacobstein, J., and Lewis, K.E. (2008). Zebrafish V2 cells develop into excitatory CiD and Notch signalling dependent inhibitory VeLD interneurons. Dev. Biol. *322*, 263–275.

23. Cau, E., Quillien, A., and Blader, P. (2008). Notch resolves mixed neural identities in the zebrafish epiphysis. Development *135*, 2391–2401.

24. Del Barrio, M.G., Taveira-Marques, R., Muroyama, Y., Yuk, D.I., Li, S., Wines-Samuelson, M., Shen, J., Smith, H.K., Xiang, M., Rowitch, D., and Richardson, W.D. (2007). A regulatory network involving Foxn4, Mash1 and delta-like 4/Notch1 generates V2a and V2b spinal interneurons from a common progenitor pool. Development *134*, 3427–3436.

25. Peng, C.Y., Yajima, H., Burns, C.E., Zon, L.I., Sisodia, S.S., Pfaff, S.L., and Sharma, K. (2007). Notch and MAML signaling drives Scl-dependent interneuron diversity in the spinal cord. Neuron *53*, 813–827.

26. Shin, J., Poling, J., Park, H.C., and Appel, B. (2007). Notch signaling regulates neural precursor allocation and binary neuronal fate decisions in zebrafish. Development *134*, 1911–1920.

27. Ninov, N., Borius, M., and Stainier, D.Y. (2012). Different levels of Notch signaling regulate quiescence, renewal and differentiation in pancreatic endocrine progenitors. Development *139*, 1557–1567.

28. Parsons, M.J., Pisharath, H., Yusuff, S., Moore, J.C., Siekmann, A.F., Lawson, N., and Leach, S.D. (2009). Notch-responsive cells initiate the secondary transition in larval zebrafish pancreas. Mech. Dev. *126*, 898–912.

29. Bardin, A.J., Le Borgne, R., and Schweisguth, F. (2004). Asymmetric localization and function of cell-fate determinants: a fly's view. Curr. Opin. Neurobiol. *14*, 6–14.

30. Cayouette, M., Whitmore, A.V., Jeffery, G., and Raff, M. (2001). Asymmetric segregation of Numb in retinal development and the influence of the pigmented epithelium. J. Neurosci. *21*, 5643–5651.

31. Kechad, A., Jolicoeur, C., Tufford, A., Mattar, P., Chow, R.W.Y., Harris, W.A., and Cayouette, M. (2012). Numb is required for the production of terminal asymmetric cell divisions in the developing mouse retina. J. Neurosci. *32*, 17197–17210.

32. Geling, A., Steiner, H., Willem, M., Bally-Cuif, L., and Haass, C. (2002). A gamma-secretase inhibitor blocks Notch signaling in vivo and causes a severe neurogenic phenotype in zebrafish. EMBO Rep. *3*, 688–694.

33. Scheer, N., and Campos-Ortega, J.A. (1999). Use of the Gal4-UAS technique for targeted gene expression in the zebrafish. Mech. Dev. *80*, 153–158.

34. Bernardos, R.L., and Raymond, P.A. (2006). GFAP transgenic zebrafish. Gene Expr. Patterns *6*, 1007–1013.

35. Garcia, A.D., Doan, N.B., Imura, T., Bush, T.G., and Sofroniew, M.V. (2004). GFAP-expressing progenitors are the principal source of constitutive neurogenesis in adult mouse forebrain. Nat. Neurosci. *7*, 1233–1241.

36. Bernardos, R.L., Lentz, S.I., Wolfe, M.S., and Raymond, P.A. (2005). Notch-Delta signaling is required for spatial patterning and Müller glia differentiation in the zebrafish retina. Dev. Biol. *278*, 381–395.

37. Furukawa, T., Mukherjee, S., Bao, Z.Z., Morrow, E.M., and Cepko, C.L. (2000). rax, Hes1, and notch1 promote the formation of Müller glia by postnatal retinal progenitor cells. Neuron *26*, 383–394.

38. Jadhav, A.P., Cho, S.H., and Cepko, C.L. (2006). Notch activity permits retinal cells to progress through multiple progenitor states and acquire a stem cell property. Proc. Natl. Acad. Sci. USA *103*, 18998–19003.

39. Scheer, N., Groth, A., Hans, S., and Campos-Ortega, J.A. (2001). An instructive function for Notch in promoting gliogenesis in the zebrafish retina. Development *128*, 1099–1107.

40. Riepe, R.E., and Norenburg, M.D. (1977). Müller cell localisation of glutamine synthetase in rat retina. Nature *268*, 654–655.

41. Dullin, J.P., Locker, M., Robach, M., Henningfeld, K.A., Parain, K., Afelik, S., Pieler, T., and Perron, M. (2007). Ptf1a triggers GABAergic neuronal cell fates in the retina. BMC Dev. Biol. *7*, 110.

42. Fujitani, Y., Fujitani, S., Luo, H., Qiu, F., Burlison, J., Long, Q., Kawaguchi, Y., Edlund, H., MacDonald, R.J., Furukawa, T., et al. (2006). Ptf1a determines horizontal and amacrine cell fates during mouse retinal development. Development *133*, 4439–4450.

43. Jusuf, P.R., Almeida, A.D., Randlett, O., Joubin, K., Poggi, L., and Harris, W.A. (2011). Origin and determination of inhibitory cell lineages in the vertebrate retina. J. Neurosci. *31*, 2549–2562.

44. Lelièvre, E.C., Lek, M., Boije, H., Houille-Vernes, L., Brajeul, V., Slembrouck, A., Roger, J.E., Sahel, J.A., Matter, J.M., Sennlaub, F., et al. (2011). Ptf1a/Rbpj complex inhibits ganglion cell fate and drives the specification of all horizontal cell subtypes in the chick retina. Dev. Biol. *358*, 296–308.

45. Nakhai, H., Sel, S., Favor, J., Mendoza-Torres, L., Paulsen, F., Duncker, G.I., and Schmid, R.M. (2007). Ptf1a is essential for the differentiation of GABAergic and glycinergic amacrine cells and horizontal cells in the mouse retina. Development *134*, 1151–1160.

46. Lin, J.W., Biankin, A.V., Horb, M.E., Ghosh, B., Prasad, N.B., Yee, N.S., Pack, M.A., and Leach, S.D. (2004). Differential requirement for ptf1a in endocrine and exocrine lineages of developing zebrafish pancreas. Dev. Biol. *270*, 474–486.

47. Brown, N.L., Kanekar, S., Vetter, M.L., Tucker, P.K., Gemza, D.L., and Glaser, T. (1998). Math5 encodes a murine basic helix-loop-helix transcription factor expressed during early stages of retinal neurogenesis. Development *125*, 4821–4833.

48. Kanekar, S., Perron, M., Dorsky, R., Harris, W.A., Jan, L.Y., Jan, Y.N., and Vetter, M.L. (1997). Xath5 participates in a network of bHLH genes in the developing Xenopus retina. Neuron *19*, 981–994.

49. Kay, J.N., Finger-Baier, K.C., Roeser, T., Staub, W., and Baier, H. (2001). Retinal ganglion cell genesis requires lakritz, a Zebrafish atonal Homolog. Neuron *30*, 725–736.

50. Liu, W., Mo, Z., and Xiang, M. (2001). The Ath5 proneural genes function upstream of Brn3 POU domain transcription factor genes to promote retinal ganglion cell development. Proc. Natl. Acad. Sci. USA *98*, 1649–1654.

51. Masai, I., Stemple, D.L., Okamoto, H., and Wilson, S.W. (2000). Midline signals regulate retinal neurogenesis in zebrafish. Neuron *27*, 251–263.

52. Pittman, A.J., Law, M.Y., and Chien, C.B. (2008). Pathfinding in a large vertebrate axon tract: isotypic interactions guide retinotectal axons at multiple choice points. Development *135*, 2865–2871.

53. Mizeracka, K., DeMaso, C.R., and Cepko, C.L. (2013). Notch1 is required in newly postmitotic cells to inhibit the rod photoreceptor fate. Development *140*, 3188–3197.

54. Cox, B.C., Chai, R., Lenoir, A., Liu, Z., Zhang, L., Nguyen, D.H., Chalasani, K., Steigelman, K.A., Fang, J., Rubel, E.W., et al. (2014). Spontaneous hair cell regeneration in the neonatal mouse cochlea in vivo. Development *141*, 816–829.

55. McGovern, M.M., Zhou, L., Randle, M.R., and Cox, B.C. (2018). spontaneous hair cell regeneration is prevented by increased Notch signaling in supporting cells. Front. Cell. Neurosci. *12*, 120.

56. Poggi, L., Vitorino, M., Masai, I., and Harris, W.A. (2005). Influences on neural lineage and mode of division in the zebrafish retina in vivo. J. Cell Biol. *171*, 991–999.

57. Gascón, S., Masserdotti, G., Russo, G.L., and Götz, M. (2017). Direct neuronal reprogramming: achievements, hurdles, and new roads to success. Cell Stem Cell *21*, 18–34.

58. Jorstad, N.L., Wilken, M.S., Grimes, W.N., Wohl, S.G., VandenBosch, L.S., Yoshimatsu, T., Wong, R.O., Rieke, F., and Reh, T.A. (2017). Stimulation of functional neuronal regeneration from Müller glia in adult mice. Nature *548*, 103–107.

59. Mattugini, N., Bocchi, R., Scheuss, V., Russo, G.L., Torper, O., Lao, C.L., and Götz, M. (2019). Inducing different neuronal subtypes from astrocytes in the injured mouse cerebral cortex. Neuron *103*, 1086–1095.e5.

60. Kimura, Y., Okamura, Y., and Higashijima, S. (2006). alx, a zebrafish homolog of Chx10, marks ipsilateral descending excitatory interneurons that participate in the regulation of spinal locomotor circuits. J. Neurosci. *26*, 5684–5697.

61. Williams, P.R., Suzuki, S.C., Yoshimatsu, T., Lawrence, O.T., Waldron, S.J., Parsons, M.J., Nonet, M.L., and Wong, R.O. (2010). In vivo development of outer retinal synapses in the absence of glial contact. J. Neurosci. *30*, 11951–11961.

62. Scott, E.K., Mason, L., Arrenberg, A.B., Ziv, L., Gosse, N.J., Xiao, T., Chi, N.C., Asakawa, K., Kawakami, K., and Baier, H. (2007). Targeting neural circuitry in zebrafish using GAL4 enhancer trapping. Nat. Methods *4*, 323–326.

63. Heap, L.A., Goh, C.C., Kassahn, K.S., and Scott, E.K. (2013). Cerebellar output in zebrafish: an analysis of spatial patterns and topography in eurydendroid cell projections. Front. Neural Circuits *7*, 53.

64. Girdler, G.C., Araya, C., Ren, X., and Clarke, J.D. (2013). Developmental time rather than local environment regulates the schedule of epithelial polarization in the zebrafish neural rod. Neural Dev. *8*, 5.

65. Reugels, A.M., Boggetti, B., Scheer, N., and Campos-Ortega, J.A. (2006). Asymmetric localization of Numb:EGFP in dividing neuroepithelial cells during neurulation in Danio rerio. Dev. Dyn. *235*, 934–948.

66. Schindelin, J., Arganda-Carreras, I., Frise, E., Kaynig, V., Longair, M., Pietzsch, T., Preibisch, S., Rueden, C., Saalfeld, S., Schmid, B., et al. (2012). Fiji: an open-source platform for biological-image analysis. Nat. Methods *9*, 676–682.

67. Mullins, M.C., Hammerschmidt, M., Haffter, P., and Nüsslein-Volhard, C. (1994). Large-scale mutagenesis in the zebrafish: in search of genes controlling development in a vertebrate. Curr. Biol. *4*, 189–202.

68. Kimmel, C.B., Ballard, W.W., Kimmel, S.R., Ullmann, B., and Schilling, T.F. (1995). Stages of embryonic development of the zebrafish. Dev. Dyn. *203*, 253–310.

69. Ren, J.Q., McCarthy, W.R., Zhang, H., Adolph, A.R., and Li, L. (2002). Behavioral visual responses of wild-type and hypopigmented zebrafish. Vision Res. *42*, 293–299.

70. King, A.C., Gut, M., and Zenker, A.K. (2020). Shedding new light on early sex determination in zebrafish. Arch. Toxicol. *94*, 4143–4158.

71. Kawakami, K. (2004). Transgenesis and gene trap methods in zebrafish by using the Tol2 transposable element. Methods Cell Biol. *77*, 201–222.

72. Engerer, P., Plucinska, G., Thong, R., Trovò, L., Paquet, D., and Godinho, L. (2016). Imaging Subcellular Structures in the Living Zebrafish Embryo. J. Vis. Exp. (110), e53456.

STAR★METHODS

KEY RESOURCES TABLE

REAGENT or RESOURCE	SOURCE	IDENTIFIER
Antibodies		
Mouse monoclonal anti-c-myc, clone 9E10, 1:100	Sigma-Aldrich	Cat# M5546; RRID: AB_260581
Chicken polyclonal anti-GFP, 1:1000	Abcam	Cat# ab13970; RRID: AB_300798
Mouse monoclonal anti-glutamine synthetase, clone GS-6, 1:50	Sigma-Aldrich	Cat# MAB302; RRID: AB_2110656
Goat anti-mouse Alexa 647, IgG1, 1:250	Invitrogen	Cat# A-21240; RRID: AB_141658
Goat anti-chicken Alexa 488, IgG (H+L), 1:250	Invitrogen	Cat# A-11039; RRID: AB_142924
Goat anti-mouse Alexa 568, IgG2a, 1:250	Invitrogen	Cat# A-21134; RRID: AB_2535773
Chemicals, peptides, and recombinant proteins		
N-[N-(3,5-Difluorophenacetyl)-L-alanyl]-S-phenylglycine t-butyl ester (DAPT)	Enzo Life Science	Cat# 50-200-8542
Critical commercial assays		
MyTaq Extract-PCR kit	Bioline	Cat# BIO-21126
Omniscript RT kit	QIAGEN	Cat# 205111
Ambion mMessage mMachine kit	Thermo Fisher Scientific	Cat# AM1340
Experimental models: Organisms/strains		
Zebrafish: Tg(vsx1:GFP)nns5: nns5Tg	[12,16]	ZFIN: ZDB-ALT-090116-1
Zebrafish: Tg(vsx2:GFP)nns1: nns1Tg	[12,60]	ZFIN: ZDB-ALT-061204-2
Zebrafish: Tg(UAS:gap43-YFP)q16b: q16Tg	[61]	ZFIN: ZDB-ALT-071129-3
Zebrafish: Tg(crx:MA-CFP)q20: q20Tg	[21]	ZFIN: ZDB-ALT-131118-1
Zebrafish: Tg(vsx1:Gal4)q32: q32Tg	[14]	ZFIN: ZDB-ALT-170831-2
Zebrafish: Tg(14xUAS:memTagRFP-T)	[14]	ZFIN: ZDB-ALT-170831-1
Zebrafish: Tg(ptf1a:eGFP)jh1: jh1Tg	[19]	ZFIN: ZDB-ALT-070531-2
Zebrafish: Tg(UAS:myc-notch-intra): kca3Tg	[33]	ZFIN: ZDB-ALT-020918-8
Zebrafish: Tg(T2KTp1bglob:hmgb1mCherry) jh11: jh11Tg	[28]	ZFIN: ZDB-ALT-101006-1
Zebrafish: Tg(*gfap*:GFP)mi2001: mi2001Tg	[34]	ZFIN: ZDB-ALT-060623-4
Zebrafish: Tg(UAS:Kaede)s1999t: s1999tTg	[62]	ZFIN: ZDB-ALT-070314-1
Zebrafish: Tg(−17.6isl2b:GFP): zc7Tg	[52]	ZFIN: ZDB-ALT-100322-2
Zebrafish: Tg(−1.8ctbp2:gap43-EGFP) lmb1: lmb1Tg	[20]	ZFIN: ZDB-ALT-120320-3
Zebrafish: Tg(EPV.TP1-Mmu.Hbb: hist2h2l-mCherry)s939: s939Tg	[27]	ZFIN: ZDB-ALT-110503-3
Zebrafish: Tg(14xUAS:mCherry)s1984t: s1984tTg	[63]	ZFIN: ZDB-ALT-130702-1
Zebrafish: Tg(5xUAS:Atoh7)	This paper	N/A
Zebrafish: Tg(5xUAS:Ptf1a)	This paper	N/A
Oligonucleotides		
For all primers used in cloning, see Table S1	Metabion	N/A
For all primers used in genotyping, see Table S2	Metabion	N/A
Morpholino p53: 5′- GCGCCATT GCTTTGCAAGAATTG-3′	Gene tools,[64]	ZFIN: ZDB-MRPHLNO-070126-7
Morpholino:MO1-ptf1a: 5′-CCAACA CAGTGTCCATTTTTTGTGC-3′	Gene tools,[43,46]	ZFIN: ZDB-MRPHLNO-070531-6
Recombinant DNA		
pCH-5xUAS:Ptf1a	This paper	N/A
pCH-5xUAS:Atoh7	This paper	N/A

(*Continued on next page*)

Continued		
REAGENT or RESOURCE	SOURCE	IDENTIFIER
atoh7 cDNA, I.M.A.G.E. clone	Source Bioscience	Cat# IRBVp5006D093D
pCS2 Numb-GFP	[65]	N/A
Software and algorithms		
ImageJ/Fiji	[66]	RRID: SCR_002285 ; https://fiji.sc/
Imaris	Bitplane	RRID: SCR_007370; https://imaris.oxinst.com/
Adobe Illustrator	Adobe	RRID: SCR_010279; https://www.adobe.com/
Adobe Photoshop	Adobe	RRID: SCR_014199; https://www.adobe.com/
GraphPad Prism	Graphpad Software	RRID: SCR_002798; https://www.graphpad.com

RESOURCE AVAILABILITY

Lead Contact

Further information and requests for resources and reagents should be directed to and will be fulfilled by the Lead Contact, Leanne Godinho (leanne.godinho@tum.de).

Materials Availability

Plasmids are available upon request to the lead contact.

Data and Code Availability

- All data reported in this paper will be shared by the lead contact upon request.
- This paper does not report original code.
- Any additional information required to reanalyze the data reported in this paper is available from the lead contact upon request.

EXPERIMENTAL MODEL AND SUBJECT DETAILS

Experiments were performed according to local regulations (Regierung von Oberbayern). Zebrafish were maintained and bred as previously described.[67] Embryos were kept in 0.3x Danieau's solution at 28.5°C and staged as previously described.[68] Fish were either in an AB wild-type, Tuebingen Long Fin (TLN) or roy orbison[69] background. All experiments were performed on animals between 2 and 5 days post fertilization (dpf). During this period zebrafish are not sexually differentiated.[70] The transgenic lines used are listed in the key resources table. Note that line Tg(*vsx1*:Gal4)q32 (*Q32*) was referred to as Tg(*vsx1*:Gal4)q26 (*Q26*).[14] To generate the line, a 3.2 kb fragment upstream of the *vsx1* coding sequence was used to drive the expression of Gal4-VP16. Crossing the *Q32*:Gal4 line, in conjunction with a *uas*:memTag-RFP-T line, to *vsx1*:GFP revealed that the *Q32* driver faithfully labels a subset of *vsx1*:GFP+ cells.[14] We generated Tg(*5xuas*:Ptf1a) and Tg(*5xuas*:Atoh7) by Tol2 mediated insertion.[71]

METHOD DETAILS

Generation of constructs

To generate *pCH-5xuas*:Atoh7, the coding sequence of zebrafish *atoh7* (*atonal bHLH transcription factor 7*) was PCR amplified using primers containing EcoRI and NotI restriction sites (sequences of primers Atoh7 Forward and Atoh7 Reverse are available in Table S1) from a plasmid containing full-length *atoh7* cDNA (I.M.A.G.E Clone IRBVp5006D093D, Source Bioscience). The amplified *atoh7* sequence was cloned into a *5xuas* backbone using EcoRI and NotI. The *5xuas* backbone was generated by excising TagRFP-T out of *5xuas*:TagRFP-T (gift from Dr. M. Meyer, King's College, London, UK) using EcoRI and NotI. Subsequently, *5xuas*:Atoh7 was excised with AseI and AflII and ligated into the pColdHeart Tol2 vector (gift from Dr. M. Nonet, Washington University, St. Louis, USA) using blunted NheI and ClaI restriction sites.

To generate *pCH-5xuas*:Ptf1a, the coding sequence of zebrafish *ptf1a* was amplified using primers containing XmaI and NotI restriction sites (sequences of primers Ptf1a Forward and Pf1a Reverse in Table S1) from zebrafish cDNA (obtained by reverse transcription, Omniscript RT kit, QIAGEN) and cloned into the *5xuas* backbone using XmaI/NotI. *5xuas*:Ptf1a was released with AseI and AflII and ligated into the pColdHeart Tol2 vector using blunted NheI and ClaI restriction sites.

Capped RNA synthesis and injections

The PCS2 Numb-GFP plasmid was linearized using NotI. Capped mRNA was synthesized using the Ambion mMessage mMachine kit (Applied Biosystems) according to the manufacturer's instructions. Numb RNA was injected in one- to two-cell stage fertilized eggs at a concentration of 20ng/μl.

Mounting zebrafish larvae for *in vivo* imaging

Embryos were prepared for imaging as described previously.[14,72] Between 10 and 24 h post-fertilization (hpf), embryos were transferred to 0.3 × Danieau's solution containing 0.003% 1-phenyl-2-thiourea (PTU, Sigma) to inhibit melanin formation. Embryos were manually dechorionated (when necessary), anesthetized using 0.02% tricaine (PharmaQ) in medium containing PTU and embedded laying on their side in low-melting agarose (0.7%–0.8%, Sigma) in glass covered 35mm dishes (MatTek, P35G-0-14-C).

In vivo imaging

Fish were imaged on an Olympus FV1000 confocal/2-photon, Olympus FVMPE-RS 2-photon, Olympus FV3000 or a Leica TCS SP8 microscope using water-immersion objectives (Olympus 20x/NA 0.95, Olympus 25x/NA 1.05, Zeiss 40x/NA 1.0, Nikon 25x/NA 1.1 and Nikon 40x/NA 0.8, Leica 25x/NA 0.95) or a silicon-immersion objective (Olympus 30x/NA 1.05). Embryos were maintained at 28.5°C during *in vivo* time-lapse recordings.

Photoconversion

The 'tornado scan' function on an Olympus FV1000 confocal was used to photoconvert Kaede in a local patch of *Q32* cells within the INL of *Q32*; *uas*:Kaede double transgenic fish with a 405 nm laser. Retinae were imaged immediately following photoconversion (Day 0). Fish were then unmounted from agarose and maintained in the dark at 28.5°C until subsequent imaging time-points at 24h (Day 1) and 48h (Day 2).

Morpholino injections

An antisense *ptf1a* translation-blocking morpholino (0.5mM, MO1, Gene tools, for sequence see key resources table), was injected using a picospritzer into the yolk of one or two-cell stage compound transgenic embryos (*Q32*; mYFP; NICD; Atoh7). A *p53* morpholino (0.02 to 1.0 mM, Gene tools, for sequence see key resources table) was injected into embryos from the *vsx1*:GFP line that were subsequently treated at 2 dpf with DAPT (see below).

DAPT treatment

N-[N-(3,5-Difluorophenacetyl)-L-alanyl]-S-phenylglycine t-butyl ester (DAPT) was used at a final concentration of 50 μM in 0.3x Danieau's containing 1% DMSO. Embryos were injected with a *p53* morpholino to ameliorate DAPT induced toxicit.[64] At 2 dpf, embryos were transferred into DAPT containing medium (or DMSO containing medium as a control) and incubated for approximately 20 h before analysis.

Immunostaining

Immunostaining to detect glutamine synthetase, c-*myc* and YFP was performed on whole-mount compound transgenic embryos. Zebrafish embryos were fixed in 4% (wt/vol) paraformaldehyde (PFA) in 1x PBS at 4°C overnight. Following fixation, embryos were washed (3x5min) in 1x PBS, pH 7.4, and then incubated in 0.25% Trypsin in 1x PBS on ice for 3-4 min. Embryos were then washed 3-4 times in 1x PBS and incubated in 0.4% Blocking Reagent (Roche) in PBS for 1.5h. Incubation in primary antibodies, diluted in 1x PBS containing 1% Triton (PBST) and 0.4% Blocking reagent, proceeded for two days at 4°C. Following several washes in PBST for 4-5h, embryos were incubated in appropriate Alexa dye-coupled secondary antibodies overnight at 4°C in 0.4% Blocking reagent in PBST. Following several washes in 1x PBS, embryos were mounted in low-melting agarose (0.7%–0.8%, Sigma) and imaged. All incubation and washing steps were done on a rotating shaker.

Genotyping of Q32 crosses

The presence of the *uas*:NICD transgene was initially determined by immunostaining for the c-*myc* tag (99.1 ± 0.6% of YFP^+ cells were c-myc^+; 428 cells, 3 *Q32* NICD fish). The presence of c-*myc* staining correlated perfectly with exuberant neuritic arbors and the loss of lamination in the IPL as well as supernumerary ACs in retinae from putative *Q32* NICD fish (12 out of 12 fish). Thus, the presence of the NICD transgene could be readily determined by retinal morphology. The presence of the *uas*:Ptf1a or *uas*:Atoh7 transgene in embryos could be confirmed by cyan fluorescence in the heart as both constructs were generated using the pCold-Heart Tol2 vector in which *cmcl2* promoter elements drive the expression of CFP.

For some experiments we genotyped individual embryos after confocal imaging to definitively identify carriers of the *uas*:NICD or *uas*:Atoh7 transgenes. Between 6-11dpf, fish were anesthetized in 0.2% tricaine (PharmaQ) and processed for genotyping. DNA extraction was performed using a MyTaq Extract-PCR kit (Bioline, BIO-21126) according to the Manufacturer's guidelines. In brief, each reaction required 20μl Buffer A, 10μl Buffer B and 70μl Nuclease-Free Water (Ambion). Each larva was placed into a clean 1.5ml tube and the extraction mix was added. The reaction was incubated for 75°C for 5-6min and vortexed at least twice. Enzymatic deactivation was achieved by heating to 95°C for 10min followed by centrifugation at 14000rpm for 5min. The genomic DNA of each individual larva was transferred to a clean 1.5ml tube and used as a template for the genotyping. PCR to detect the transgenes used OneTaq hot Start DNA Polymerase (NEB, M0481) along with primers to detect Actin as a proxy to determine the integrity of the genomic DNA. Primers used for genotyping are listed in Table S2.

QUANTIFICATION AND STATISTICAL ANALYSIS

Cell type classification of Q32 cells

Q32 cells were classified as BC or AC based on neurite morphology (presence or absence respectively of an apical process) and position of the soma (lower or upper half of the INL). To obtain the AC-BC ratio of different *Q32* genotypes, a maximum intensity projection (MIP) of a few imaging planes (typically 5) was obtained, and all *Q32* cells (at least 70 per retina) in the MIP were classified. *Q32* divisions were classified as BC-BC, AC-BC or AC-AC based on the criteria described above.

Quantification of Kaede recovery in photoconverted Q32 cells

The recovery of green fluorescence intensity of Kaede protein (I_{CV}) was measured in a region of interest (ROI) encompassing the soma of individual BCs and ACs in a single image plane of a confocal stack and the background fluorescence (I_{BG}) averaged from six regions (*Q32* negative) was subtracted to correct for auto-fluorescence and potential out-of-focus contributions. In order to compare across different samples, fluorescence intensity values were normalized to the average fluorescence intensity of 6 unconverted BCs (I_{UC}) from the same section. The recovery of green fluorescent Kaede protein in *Q32* BCs and ACs was expressed as a percentage:

$$\textit{Recovery of green fluorescence in Q32 BC} = \frac{I_{CV\_BC} - I_{BG}}{I_{UC\_BCs} - I_{BG}}\%$$

$$\textit{Recovery of green fluorescence in Q32 AC} = \frac{I_{CV\_AC} - I_{BG}}{I_{UC\_BCs} - I_{BG}}\%$$

The unconverted BCs were chosen in the vicinity of the photoconverted area and ± 5 sections from the depth in which the photoconverted area was in focus. The same procedure was followed to obtain background values.

Analysis of DAPT treated animals

The effect of DAPT treatment was quantified in two independent quadrants of the peripheral retina of *vsx1*:GFP fish. In a given quadrant, the total number of *vsx1*:GFP^{+} ACs were counted in 10 z-planes.

Notch-Reporter levels in differentiated Q32 cells

Tp1:hmgb1mCherry fluorescence intensity levels were determined in *Q32* ACs and their potential sibling BCs. If at least one of the *Q32* cells had a fluorescence intensity level twice above background, the cell group was used for analysis (34/77 cell groups could be used). To classify a cell group as 'AC high', 'BC high' or 'equal', Notch-Reporter levels in the *Q32* AC were compared to the surrounding *Q32* BCs with the highest Notch-Reporter fluorescence. If the *Q32* AC had twice the brightness of the *Q32* BC, the group was classified as 'AC high'. Similarly, in cases in which the *Q32* BC had twice the brightness of the *Q32* AC, the group was classified as 'BC high'. When no cell had at least twice the fluorescence intensity of the other, the group was classified as 'equal'.

Monitoring Notch-Reporter levels in time-lapse recordings of the Q32 lineage

Tp1:H2BmCherry fluorescence intensity levels were monitored in the *Q32* lineage by *in vivo* imaging. *Q32* BC-AC pairs were identified and their somata were manually demarcated based on their mYFP expression in a single image plane of a confocal stack using the ImageJ freehand tool. Notch-Reporter levels were measured based on the fluorescence intensity of the mCherry channel within the demarcated areas. The same approach was used for *Q32* transdifferentiation events in the NICD OE condition. Background values (mCherry channel) from three areas at the same time point were averaged and subtracted from the fluorescence intensity values of the cells being measured. Contributions of fluorescence from cells outside of the *Q32* lineage were identified as moving ''objects'' and used to correct the demarcation of each cell of interest accordingly. Finally, the fluorescence values were normalized to the time point before mitosis for the *Q32* BC-AC siblings or to the first time point seen for the transdifferentiation events after background subtraction.

Division rate analysis

The number of mitotic divisions in the *Q32* lineage in WT and NICD OE, irrespective of their outcome (BC-AC or BC-BC), were counted over a time span of ~18h between 52 hpf and 70 hpf. The division rate was expressed as the total number of divisions per hour.

Cleavage plane analysis

The cleavage planes of dividing progenitors that ultimately generated BC-AC daughters were analyzed. Cell divisions were analyzed in imaging volumes with a reference to the apical surface. Divisions were classified as apico-basal if the cells divided perpendicular to the apical surface and both siblings were present in the same imaging plane. Circumferential divisions occurred parallel to the apical surface and when both siblings were present in the same imaging plane. Central-peripheral divisions also occurred parallel to the

apical surface but the two cells were at different z-depths (larger than 2.4 μm) representing the central-peripheral axis of the retina. When dividing cells could not be strictly categorized in these three categories we ascribed them to an intermediate class.

Statistics

The Shapiro-Wilk test was used to determine whether parametric or non-parametric tests were appropriate for determining statistical significance with GraphPad Prism 8. The specific statistical tests used to compare data-sets are indicated in the respective part of the text or figure legend. $P \leq 0.05$ denoted with '*', ≤ 0.01 with '**', ≤ 0.001 with '***', ≤ 0.0001 ****.